A miniature LiDAR with a detached MEMS scanner for micro-robotics

Dingkang Wang, Huikai Xie, *Fellow, IEEE*, Lenworth Thomas, and Sanjeev Koppal, *Senior Member, IEEE*

***Abstract*—Light detection and ranging (LiDAR) has been widely used for airborne surveillance and autonomous driving. The ability of robotics or even micro-robotics can be drastically enhanced if equipped with LiDAR, but very light and small LiDAR must be used. Micro-robots have sizes close to birds or insects, and almost all existing LiDAR are too heavy and too large for them. In this work, a novel MEMS LiDAR, with its optical scanner separated from its base, is proposed and demonstrated. The scanner head will be carried by a moving micro-robot while the LiDAR base is fixed on the ground. There is a thin, flexible optical/electrical cable connecting the scanner head to the base. The scanner head consists of a MEMS mirror and a rod lens, which weighs only 10 g and measures under 4 cm long. The MEMS mirror has an aperture of 1.2 mm × 1.4 mm and can scan a field of view (FoV) of 9° × 8°. As the micro-robot and the optical scanner head moves with respect to the optical receiver, an IMU (inertial measurement unit) has been embedded in the scanner head to track the motion and an algorithm has been developed to reconstruct the true point clouds. The movable head LiDAR can acquire 400 points per second and detect targets up to 35 cm away. A micro-robot can carry the scanner head while it is moving, and the point clouds can be generated at the LiDAR base. This new LiDAR configuration enables ranging, mapping, tracking, and zoom-in scanning for micro-robots.**

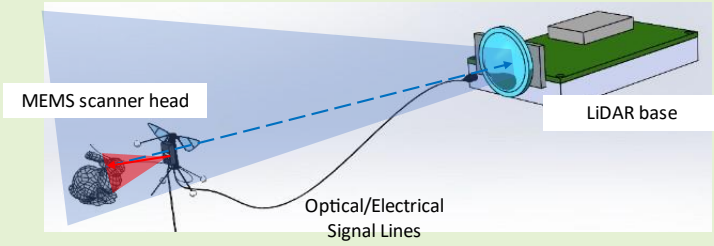

***Index Terms*— MEMS mirror, micro-robotics, electrothermal actuation, LiDAR**

I. Introduction

MICROROBOTS are intelligent systems inspired by insects and birds and have shown significant potential to conduct tasks such as surveillance, pollination, and small target delivery [1]. Currently, most microrobots use optical flow sensing or inertial measurement unit (IMU) for navigation and exploration [2][3]. Light detection and ranging (LiDAR) devices have been widely used for robotics [4]-[6]. LiDARs can make accurate dynamic distance measurements for mapping and avoiding obstacles, attracting great interest in micro-robotics [7][8]. Traditional LiDARs used in automotive vehicles typically employ motorized scanners and stacks of multiple lasers and photodetectors, so they often weigh in kilograms and measure in decimeters [9][10].

Fortunately, Micro-Electro-Mechanical Systems (MEMS) technology can be used to drastically reduce the weight and size of LiDAR scanners and build compact LiDAR systems [4][11]-[14]. For instance, Xu et al. demonstrated a MEMS-based LiDAR with a small volume of 103 mm × 90 mm × 95 mm [13]. Wang et al. developed a low-power, small-size 3D LiDAR prototype based on an electrothermal MEMS mirror [12], which had an overall size of 21 cm × 9 cm × 6.5 cm and weighed around 200 g. Mitsubishi Electric also introduced a MEMS LiDAR with dimensions of 108 mm × 105 mm × 96 mm [14]. Different from a conventional LiDAR, a MEMS mirror-based LiDAR only needs one laser transmitter to generate a 2D field of view (FoV), which significantly simplifies the LiDAR structure.

However, even equipped with a small and light-weighted MEMS mirror, a MEMS LiDAR is still too large and heavy for micro-robotics. This is because other components of the LiDAR, including the laser, photodetector, optics, and electronics, are typically much bigger and heavier than the MEMS mirror.

On the other hand, most micro-robots today still use electrical wires to deliver power due to the lack of ultra-high-density micro-batteries [1][3][17]. For example, the Robobee, an insect-like micro air vehicle (MAV) developed by Baisch and Wood [1], can fly in an enclosed space under a relatively low speed with attached electrical wires for power. With a LiDAR that can detect its surroundings, the Robobee would be able to complete many specific tasks in some narrow and dangerous environments, like finding a person buried in

Manuscript received XXX 10, 2021; XXX April 28, 2021. Date of publication XXX 14, 202`; date of current version XXX 14, 2021. This work is supported by the US Office of Naval Research and the NSF MIST Center.

Dingkang Wang and Sanjeev Koppal are with the Department of Electrical and Computer Engineering, University of Florida, Gainesville, Florida, USA (wangdk93@outlook.com; sjkoppal@ece.ufl.edu).

Huikai Xie is the corresponding author and he is with the School of Information and Electronics, Beijing Institute of Technology, Beijing, 100081, China. (hk.xie@ieee.org).

Lenworth Thomas is with the Department of Mechanical and Aerospace Engineering, University of Florida, Gainesville, FL 32603, USA (lenworth.thomas@ufl.edu).

earthquake rubbles, or surveilling a chemical-leaked room through a small window. Interestingly, in microendoscopic imaging applications, those miniature endoscopic probes rely on external light sources and photodetectors and employ optical fibers and very thin electrical wires to deliver and receive both optical and electrical signals[18]. These methods inspire the idea of an optical scanner detached (OSD) LiDAR design proposed in this work. As shown in Fig. 1, the OSD LiDAR consists of a detached optical scanning head and a fixed base module, both of which are connected by a thin, flexible cable with an optical fiber and electrical wires embedded. The optical scanning head is mainly composed of a 2-axis scanning MEMS mirror, weighs only 10 g, and has dimensions of 36 mm × 30 mm × 13 mm. The base module of the LiDAR includes the laser source and optical photodetector as well as their associated optics and electronics. As shown in Fig. 1, the key difference of this OSD LiDAR from other LiDAR systems is that the optical scanner and the laser source and photodetector are located on two different platforms. The optical scanner moves with the micro-robot carrying it while the laser source and optical receiver are fixed at the LiDAR base. Thus, an inertial measurement unit (IMU) is proposed to track the position of the optical scanner in this work.

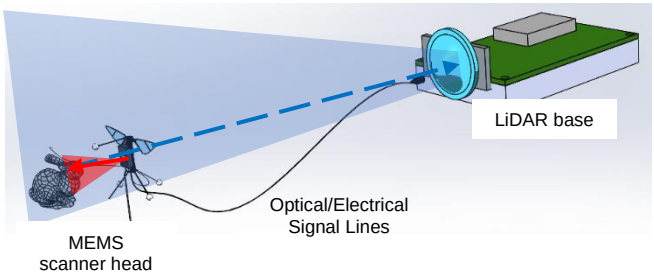

Fig. 1. Our envisioned design for micro-robots with the Robobee [1] as an example.

The detached scanner head is much smaller and lighter than the base module of the whole LiDAR and can be carried by a micro-robot. The point cloud generation algorithm of this novel LiDAR is developed. This new OSD LiDAR configuration enables ranging, mapping, tracking, and zoom-in scanning for micro-robots, and the proof-of-concept experiments are demonstrated.

II. Implementation of the MEMS-based OSD LiDAR

Fig. 2 shows the schematic design of the LiDAR with a detached MEMS scanner head. A MEMS mirror, a C-lens collimator, and an IMU (MPU9250, InvenSense) are packaged in the scanner head. A 1 m-long optical fiber delivers laser pulses to the scanner head from the laser source on the LiDAR base. Bundled with the fiber, a few thin electrical wires are routed to the scanner head to control the MEMS mirror and receive the IMU's signals.

The employed MEMS mirror is based on electrothermal bimorph actuators that are made of the inverted-series-connected (ISC) bimorph actuation structure reported in [19]. Fig. 3(b) is an SEM image of a fabricated ISC MEMS mirror. This MEMS mirror is selected to balance the trade-off between the mirror plate size and the non-resonant scanning FoV. The MEMS mirror has an optical aperture of 1.4 × 1.2 mm^2 and a non-resonant FoV of 9° (horizontal) × 8° (vertical). The scanning angle is controlled through a look-up-table method.

The laser exiting from the fiber is collimated with a C-lens collimator and an iris is used to ensure the laser beam shine only on the MEMS mirror plate. A 3D printed structure is used to assemble the MEMS mirror, C-lens, iris, and IMU altogether. A prototype of the OSD LiDAR is shown in Fig. 3(a), whose weight is about 10 g. Fig. 3(c) is a picture taken from the backside of the optical scanner head, where the IMU is visible.

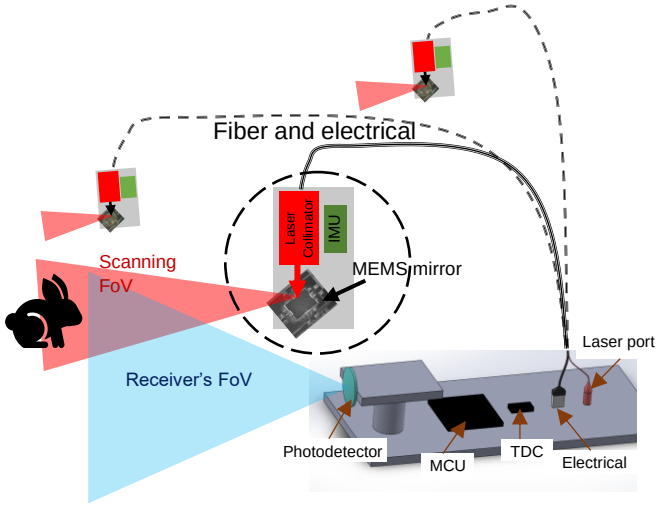

Fig. 2. The schematic of the OSD LiDAR with a detached scanner head.

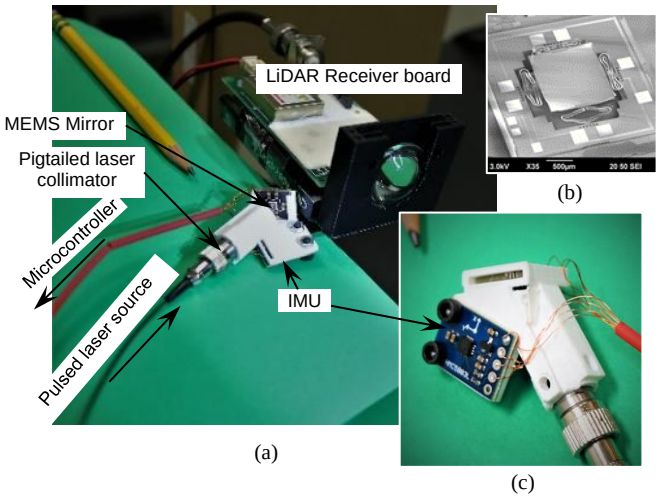

Fig. 3. (a) A prototype of the proposed LiDAR. (b) The MEMS mirror used in the LiDAR scanner. (c) Backside view of the scanner.

All other components of the OSD LiDAR are packaged in the LiDAR base, including the laser and its driver circuit, the photodetector and its optics and electronics, the MEMS driver circuit, the timing unit, and the microcontroller (MCU). The laser source is a 905 nm solid-state pulse laser (905D2S3J09R, Laser Components USA, Inc.) with a pulse width of 50 ns and a peak power of 0.6 W measured at the collimator output, while the photodetector is an APD (Avalanche Photodiode, C12702-04, Hamamatsu Inc.). A condenser lens with a diameter of 27 mm is used to increase the receiver's aperture and collect more return light, and the full acceptance angle of the receiver is 15°.

The received optical signal is amplified and sent to a comparator with a fixed threshold voltage. The analog signal is converted to a digital signal and sent to a time-to-digital converter (TDC, TDC7201, Texas Instruments) to calculate the time of flight. Two commonly used methods are adopted to improve the accuracy. First, two time-stamps at the head edge and the tail edge are measured and averaged for each return pulse to compensate for the amplitude variations. In addition, at each MEMS mirror scanning position, four laser pulses are fired, and the acquired signals are averaged to decrease the jitter. A depth accuracy of 1.5 cm is achieved. The synchronization of the timestamps of the laser trigger, the time of flight (ToF) acquisition from the TDC, and the MEMS mirror actuation are realized by the MCU.

III. Signal Processing and Position-Tracking Algorithm

The point cloud generation of the OSD LiDAR is different from those of conventional LiDAR systems. To generate the point cloud, a conventional LiDAR can simply convert the measurement data from a spherical to a Cartesian coordinate system. However, for the OSD LiDAR, the relative position and orientation between the moving scanner and the fixed photodetector are varying over time. Thus, we must consider two coordinator systems, or two frames, namely, the fixed frame **XYZ** and the moving frame **X'Y'Z'**, as illustrated in Fig. 4(a).

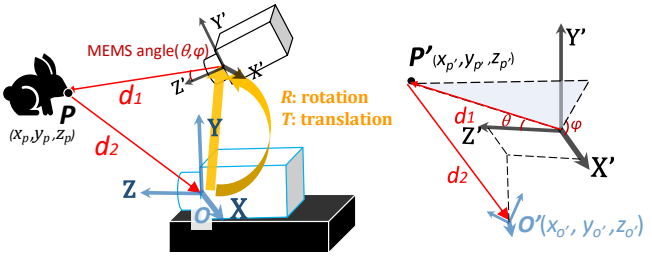

(a) (b)

Fig. 4. (a) The schematic of the relationship between the frames. (b) The point cloud seen in the moving frame **X'Y'Z'**.

XYZ is the LiDAR base reference frame and **X'Y'Z'** is the moving LiDAR scanner head frame. The origin of **XYZ** is set at the photodetector while the origin of **X'Y'Z'** is at the center of the MEMS mirror and **Z'** is perpendicular to the surface plane of the MEMS mirror chip. The IMU is placed near the MEMS mirror chip, and the primary axes of the IMU are assumed to be aligned with **X'Y'Z'**. Both rotation and translation operations are needed to transform from **XYZ** to **X'Y'Z'**, represented by the rotation matrix, $\mathbf{R}_{4\times4}$, and the translation matrix, $\mathbf{T}_{4\times4}$ [20], which can be obtained from the initial orientation and position of the MEMS mirror chip and the real-time data from the IMU or a vision-based motion tracking system.

As shown in Fig. 4(a), upon the operation of the LiDAR, the MEMS mirror scans $\theta(t)$ and $\varphi(t)$ along its rotational axes, i.e., **Z'** and **X'**, respectively, and sends a laser pulse to the target (point **P**). The laser pulse reaches the photodetector after traveling a distance d, which is equal to $d_1 + d_2$, where d_1 is the distance from the MEMS mirror to point **P** and d_2 is the distance from point **P** to the photodetector. Note that the calculated ToF distance also includes the optical path length of the optical fiber, which is a known value and can be directly subtracted.

To obtain the point cloud in the scanned field of view, we need to calculate the coordinates of **P** in the **XYZ** frame, denoted as **P** (x_p, y_p, z_p). Before that, the coordinates of **P** in the **X'Y'Z'** frame, denoted as P' ($x_{p'}$, $y_{p'}$, $z_{p'}$), must be calculated first. Assume the coordinates of point **O** in the **X'Y'Z'** frame are $x_{o'}$, $y_{o'}$, and $z_{o'}$, respectively. Then, as shown in Fig. 4(b), we have,

$$d = d_1 + d_2 \tag{1}$$

where,

$$d_1 = \sqrt{x_{p'}^2 + y_{p'}^2 + z_{p'}^2} \tag{2}$$

$$d_2 = \sqrt{(x_{p'} - x_{o'})^2 + (y_{p'} - y_{o'})^2 + (z_{p'} - z_{o'})^2} \tag{3}$$

Here d is obtained from the ToF data of the LiDAR and $x_{o'}$, $y_{o'}$ and $z_{o'}$ can be calculated using the translation and rotation matrices, i.e.,

$$\begin{bmatrix} x_{o'} \\ y_{o'} \\ z_{o'} \\ 1 \end{bmatrix} = R * T \begin{bmatrix} 0 \\ 0 \\ 0 \\ 1 \end{bmatrix} \tag{4}$$

Also, $y_{p'}$ and $z_{p'}$ can be represented by $x_{p'}$, and the scan angles of the MEMS mirror as follows,

$$y_{p'} = x_{p'} \tan\varphi \tag{5}$$

$$z_{p'} = \frac{x_{p'}}{\sin\theta} \tag{6}$$

Combining Eqs. (1)-(6), we can solve for $x_{p'}$, $y_{p'}$ and $z_{p'}$. Finally, the point cloud **P'** ($x_{p'}$, $y_{p'}$, $z_{p'}$) is transformed from the moving frame **X'Y'Z'** to **P**(x_p. y_p. z_p) in the LiDAR base reference frame **XYZ** as follows,

$$\begin{bmatrix} x_p \\ y_p \\ z_p \\ 1 \end{bmatrix} = (R * T)^{-1} \begin{bmatrix} x_{p'} \\ y_{p'} \\ z_{p'} \\ 1 \end{bmatrix} \tag{7}$$

IV. Experimental Results

The OSD LiDAR has a maximum detection range of 35 cm with a white paper as the target. The 35 cm range may be only useful for slowly moving MAVs, and a longer range is achievable by using a higher power laser. The depth accuracy at 30 cm is 1.5 cm. The error from the orientation/translation measurement will result in a distorted point cloud or a shift of the center of the point cloud. Since the maximum range is small, the distortion and shift of the point cloud are not noticeable. The errors of the translation and orientation measurement are about 0.5 cm and 0.3 cm, respectively, both of which are much smaller than the LiDAR range error.

The measurement rate of the LiDAR electronics is 400 points per second. The frame rate and the spatial resolution can be adjusted. For example, a maximum frame rate of 6.25 fps can be achieved with a spatial resolution of 8 by 8 pixels, or a

maximum spatial resolution of 20 by 20 pixels can be achieved with a slower frame rate of 1 fps.

Currently the OSD movement range is manually confined in the detector's FoV. The detector's FoV (15° by 15°) is made wider than the scanner's FoV(8° by 9°). In the future, closed-loop feedback and/or incorporation of a rotatable detector will be developed to automatically control the effective FoV.

A. Types of Graphics Zoom-in scanning with the detached optical scanner

The OSD LiDAR can perform zoom-in scanning by moving the detached scanner closer to the object of interest to improve the diffraction limit resolution. Assuming a Gaussian laser beam, the laser spot size $\omega(z)$ on the object with a distance z is given by

$$\omega(z) = \omega_0 \sqrt{1 + (\frac{z}{z_R})^2} \approx \omega_0 \frac{z}{z_R}, \quad (8)$$

where ω_0 is the beam waist, which relates to the size of the MEMS mirror plate and z_R is the Rayleigh range. The closer the scanner to the object, the smaller the laser spot size on the object is, resulting in higher transverse resolution.

For the experiment, an object (a paper fence as shown in Fig. 5(a)) is first placed 31 cm away from the scanner head and the MEMS mirror scans the area in the dashed-line box in Fig. 5(a). The resultant point cloud is shown in Fig. 5(c), where only 3-4 points are generated along the width direction of each paper board and the edges of the point cloud are noisy. Then the detached scanner head is moved closer to the paper fence at 15 cm, resulting in a smaller scanning area (the dotted-line box in Fig. 5(a)). The corresponding point cloud is shown in Fig. 5(d), where 5–6 points are present across each paper board and the edges of the point cloud become sharper.

B. Point cloud stitching with the moving scanner

The next experiment is to demonstrate the mapping capability of the OSD LiDAR. Through the fusion of the LiDAR point clouds and the states of the scanner head, multiple frames of the point cloud can be stitched together to generate a larger point cloud for mapping.

The dotted-line boxes shown in Fig. 6(a) represent different scanning FoVs of a static object. The scanner head moves and/or rotates to scan the areas outlined by the four boxes sequentially and the four corresponding point clouds are shown in Fig. 6(b). The point clouds are translated according to the motion of the scanner and are merged as shown in Fig. 6(c).

C. Tracking with the detached scanner

A mobile target may move out of a LiDAR's FoV, but most LiDARs may not be able to track rapidly moving targets. The optical scanner detached (OSD) LiDAR developed in this work can overcome this limitation. Since the detached scanner is much smaller than the LiDAR itself, this OSD LiDAR can move and rotate much faster than other LiDARs.

The paper cut in Fig. 7(a) is the object to be tracked. The paper cut is moving from position A to B, C, and D, as shown in Fig. 7(b). The scanner head is rotated and moved manually using optical posts and elevation/rotation platforms to keep the object always in the center part of the LiDAR's scanning FoV. The generated point clouds are shown next to the object in Fig. 7(b).

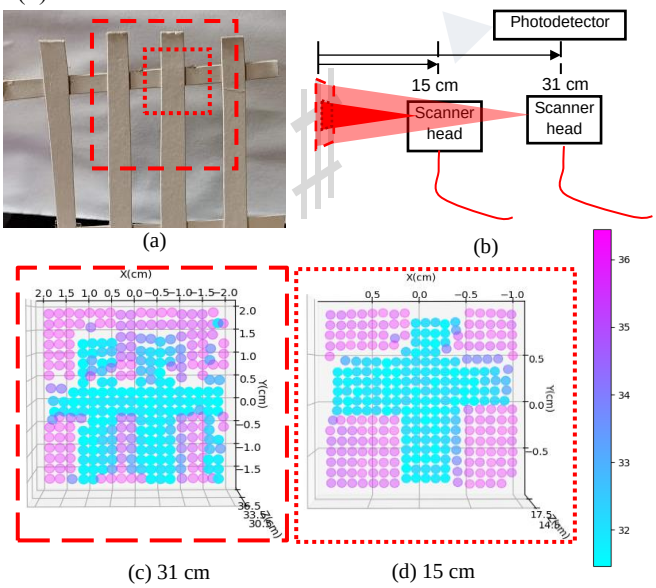

Fig. 5. (a) The test object (a paper fence) with two scanning areas outlined that correspond to two scanner positions. (b) The scanner head is 15 cm and 31 cm away, respectively. The point clouds are collected with the scanner head at 31 cm (c) and 15 cm (d) from the paper fence.

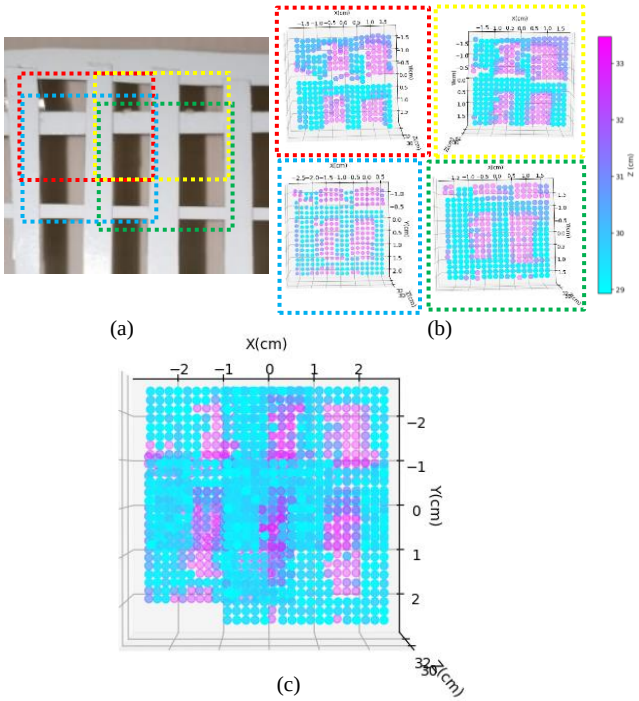

Fig. 6. (a) The target object. The four dashed boxes represent the different FoV's of the scanner head as the scanner head moves. (b) Point clouds collected at different FoV's. (c) The stitched point clouds.

There are still some limitations of this LiDAR. For example, when the detached scanner moves, the laser beam may scan out of the photodetector's FOV. This is because the photodetector is fixed toward one direction and does not move with the MEMS scanner. If the return optical signal is also collected on the movable head and fiber is used to deliver the return light to the LiDAR base, then the scanner head can move in all directions. The trade-off is the receiver's optical aperture will

be much smaller if it is on a movable head, which limits the collected light and the maximum detectable distance.

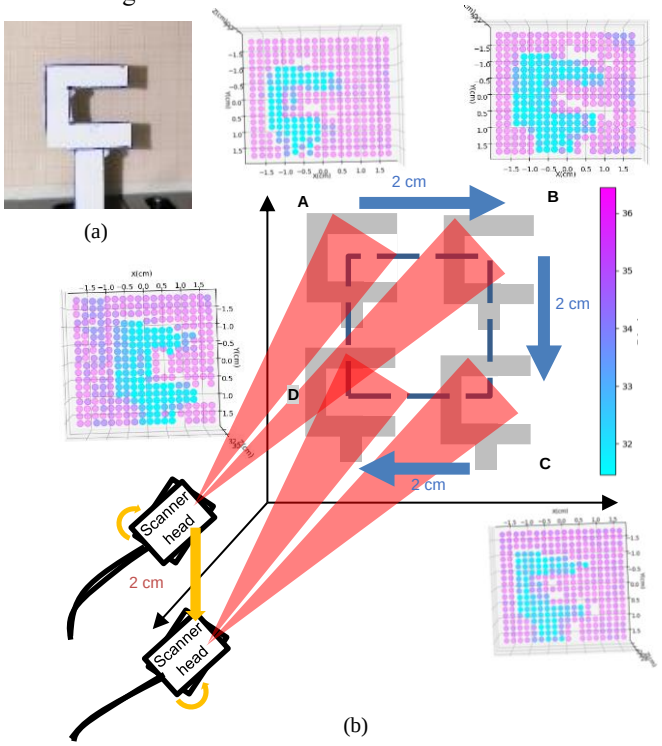

Fig. 7. (a) The target object at position A. (b) The target object is moved to position B, C and D, meanwhile the scanner head rotated/moved to make sure the object is in the LiDAR's FoV.

V. Conclusion

In this study, we have demonstrated a novel MEMS-based LiDAR with a detached optical scanner. In this optical scanner detached (OSD) LiDAR, a thin, flexible cable with an optical fiber and electrical wires embedded connects the optical scanner and a LiDAR base module. The optical scanner is mainly composed of a 2-axis MEMS mirror, weighs only 10 g, and measures 36 mm × 30 mm × 13 mm. The detached scanner is much smaller and lighter than the base module of the whole LiDAR and can be easily carried by a micro-robot. The base module of the LiDAR includes laser transmission and detection and the associated optics and electronics. An algorithm to generate point clouds for the OSD LiDAR is developed. This new LiDAR configuration enables ranging, mapping, tracking, and zoom-in scanning for micro-robots.

Acknowledgment

The authors thank the staff of the UF Research Service Centers for their assistance in the microfabrication and Yuyang Chen from the University at Buffalo for the suggestions in the Position-tracking Algorithm.

References

[1] A. T. Baisch and R. J. Wood, "Design and fabrication of the harvard ambulatory micro-robot," in *Robotics Research*, (Springer, 2011), pp. 715–730.

[2] D. S. Drew, N. O. Lambert, C. B. Schindler, and K. S. Pister, "Toward controlled flight of the ionocraft: a flying microrobot using electrohydrodynamic thrust with onboard sensing and no moving parts," *IEEE Robotics Autom. Lett*. 3, 2807–2813 (2018).

[3] R. Wood, R. Nagpal, and G.-Y. Wei, "Flight of the robobees, " *Sci. Am.* 308, 60–65 (2013).

[4] A. Kasturi, V. Milanovic, B. H. Atwood, and J. Yang, "Uav-borne lidar with mems mirror-based scanning capability," in *Laser Radar Technology and Applications XXI*, vol. 9832 (International Society for Optics and Photonics, 2016), p. 98320M.

[5] U. Weiss, and P. Biber, "Plant detection and mapping for agricultural robots using a 3D LIDAR sensor," *Robotics and autonomous systems* 59.5: 265-273 (2011).

[6] C. Sprunk, G. Tipaldi, A. Cherubini, and Burgard, W, "Lidar-based teach-and-repeat of mobile robot trajectories," in *2013 IEEE/RSJ International Conference on Intelligent Robots and Systems*, (2013), pp. 3144-3149.

[7] N. Druml, I. Maksymova, T. Thurner, D. Lierop, M. Hennecke, and A. Foroutan, "1D MEMS micro-scanning lidar," in *International Conference on Sensor Device Technologies and Applications* (SENSORDEVICES), (2018).

[8] S. Huh, S. Cho, and D. Shim, "3-D Indoor Navigation and Autonomous Flight of a Micro Aerial Vehicle using a Low-cost LIDAR," *The Journal of Korea Robotics Society* 9, no. 3 (2014): 154-159.

[9] G. Jozkow, C. Totha, and D. Grejner-Brzezinska, "UAS TOPOGRAPHIC MAPPING WITH VELODYNE LiDAR SENSOR," *ISPRS Annals of Photogrammetry, Remote Sensing & Spatial Information Sciences* 3, no. 1 (2016).

[10] R. Halterman, and M. Bruch, "Velodyne HDL-64E lidar for unmanned surface vehicle obstacle detection," in *Unmanned Systems Technology* XII, vol. 7692, (SPIE, 2010), p. 76920D.

[11] D. Wang, C. Watkins, S. Koppal, M. Li, Y. Ding, and H. Xie, "A compact omnidirectional laser scanner based on an electrothermal tripod mems mirror for lidar please leave," in *2019 20th International Conference on Solid-State Sensors, Actuators and Microsystems & Eurosensors XXXIII (TRANSDUCERS & EUROSENSORS XXXIII)*, (IEEE, 2019), pp. 1526–1529.

[12] D. Wang, L. Thomas, S. Koppal, Y. Ding, and H. Xie, "A low-voltage, low-current, digital-driven mems mirror for low-power lidar," *IEEE Sensors Lett.* 4, 1–4 (2020).

[13] F. Xu, D. Qiao, X. Song, W. Zheng, Y. He, and Q. Fan, "A semi-coaxial mems-based lidar," in *IECON 2019-45thAnnual Conference of the IEEE Industrial Electronics Society*, vol. 1 (IEEE, 2019), pp. 6726–6731.

[14] Mitsubishi ELECTRIC, "Mitsubishi Electric Develops MEMS LiDAR Solution for Autonomous Vehicles," [retrieved 18 Dec. 2020], https://www.mitsubishielectric.com/news/2020/0312.html.

[15] T. Sandner, M. Wildenhain, C. Gerwig, H. Schenk, S. Schwarzer, and H. Wölfelschneider, "Large aperture memsscanner module for 3d distance measurement," in *MOEMS and Miniaturized Systems IX*, vol. 7594 (International Society for Optics and Photonics, 2010), p. 75940D.2.

[16] E. Nunes-Pereira, P. Eduardo, J. Teixeira, and J. Santos, "The LiDAR hop-on-hop-off route: visiting the LiDARs past, present, and future landscapes," in *Fourth International Conference on Applications of Optics and Photonics*, vol. 11207, (International Society for Optics and Photonics, 2019), p. 112072Q.

[17] T. S. Clawson, S. Ferrari, S. B. Fuller, and R. J. Wood, "Spiking neural network (snn) control of a flapping insect-scale robot," in *2016 IEEE 55th Conference on Decision and Control* (CDC), (IEEE, 2016), pp. 3381–3388.

[18] H. Xie, G. K. Fedder, and Y. Pan, "MEMS-based endoscopic optical coherence tomography," in *MOEMS Display and Imaging Systems III*, vol. 5721, (International Society for Optics and Photonics, 2015), pp. 81-92.

[19] K. Jia, S. Pal, and H. Xie, "An electrothermal tip-tilt–piston micromirror based on folded dual s-shaped bimorphs," *J. Microelectromechanical systems* 18, 1004–1015 (2009).

[20] Y. Jia, "Quaternions and rotations," *Com. S.*, 477, no. 577, 15(2008).

Dingkang Wang received his B.E degree in Mechanical Engineering from Jilin University, China in 2016. He is currently working toward a Ph.D. degree in the Department of Electrical and Computer Engineering at the University of Florida, Gainesville, USA. His research interests include microelectromechanical (MEMS) systems, micro/nano fabrication, and Light Detection and Ranging (LiDAR) system.

Huikai Xie is a Professor at the School of Information and Electronics, Beijing Institute of Technology, Beijing, China. He received his BS in microelectronics, MS in photonics, and PhD in electrical and computer engineering from Beijing Institute of Technology, Tufts University, and Carnegie Mellon University, respectively. He worked at the University of Florida as an assistant professor (2002–2007), associate professor with tenure (2007–2011) and full professor (2011–2020). He has published over 300 technical papers and 11 book chapters and holds over 30 US patents. His current research interests include MEMS/NEMS, optical beam steering, optical communications, LiDAR, NIR spectroscopy, and optical microendoscopy. He is the founder of Wuxi WiO Technologies Co., Ltd. He is an associate editor of the IEEE Sensors Letters and Sensors & Actuators A. He is a fellow of IEEE and SPIE.

Lenworth Thomas was born in Orlando, Florida in 2000. He currently studies Mechanical Engineering at the University of Florida as an undergraduate student. As a recent McNair Scholar award recipient, he has been conducting research on small-scale LiDAR systems. Using his passion for cutting-edge robotics and his research experience, he hopes to pursue a PhD at a top university after he graduates.

Sanjeev J. Koppal is an assistant professor at the University of Florida ECE department. Prior to joining UF, he was a researcher at the Texas Instruments Imaging R&D lab. Sanjeev obtained his Master's and Ph.D. degrees from the Robotics Institute at Carnegie Mellon University. After CMU, he was a postdoctoral research associate in the School of Engineering and Applied Sciences at Harvard University. He received his B.S. degree from the University of Southern California in 2003. His interests span computer vision, computational photography and optics, novel cameras and sensors, 3D reconstruction, physics-based vision and active illumination.